INL/JOU-24-79019-Revision-1

Design of Mini-Plate-1 Irradiation Test for Qualification of High-Density, Low-Enriched U-10Mo Monolithic Fuel

November 2024

Seth Michael Kilby, Dong O Choe, Jason Wayne Barney, Grant L Hawkes, Colby B Jensen, Misti Lilo, Irina Glagolenko, James I Cole, Margaret A Marshall

Changing the World's Energy Future

Idaho National Laboratory

INL is a U.S. Department of Energy National Laboratory operated by Battelle Energy Alliance, LLC

INL/JOU-24-79019-Revision-1

Design of Mini-Plate-1 Irradiation Test for Qualification of High-Density, Low-Enriched U-10Mo Monolithic Fuel

Seth Michael Kilby, Dong O Choe, Jason Wayne Barney, Grant L Hawkes, Colby B Jensen, Misti Lilo, Irina Glagolenko, James I Cole, Margaret A Marshall

November 2024

Idaho National Laboratory
Idaho Falls, Idaho 83415

http://www.inl.gov

Prepared for the
U.S. Department of Energy
Under DOE Idaho Operations Office
Contract DE-AC07-05ID14517, DE-AC07-05ID14517

Design of Mini-Plate-1 Irradiation Test for Qualification of High-Density, Low-Enriched U-10Mo Monolithic Fuel

Seth M. Kilby*, Margaret A. Marshall, Dong O. Choe, Jason W. Barney, Grant L Hawkes,

Colby Jensen, Misti Lilo, Irina Y. Glagolenko, James I. Cole

Idaho National Laboratory 1955 N. Fremont Avenue Idaho Falls, ID 83415

*Corresponding author: seth.kilby@inl.gov

Abstract

The United States High Performance Research Reactor (USHPRR) project is tasked with fuel development and qualification leading to conversion of higher power research and test reactors in the United States from high-enriched uranium (HEU) to low-enriched uranium (LEU) fuels. This manuscript identifies the functional and operational design requirements of the first miniature test plate (mini-plate [MP]) irradiation campaign (MP-1) of commercially fabricated LEU U-10Mo monolithic plate-type fuel and is the precursor to a large parametric mini-plate test (MP-2) aimed at producing the data to support regulatory qualification of the LEU U-10Mo monolithic fuel. The manuscript (a) provides a general description of the selected U–10Mo LEU fuel, and (b) defines the overall experiment design and functional requirements to accomplish the specific test objective of MP-1, which is to confirm that the commercially manufactured LEU U-10Mo monolithic fuel meets the established requirements of geometric stability, mechanical integrity and stable and predictable behavior. The fuel testing parameters are established by the need to bound performance behavior within the operational envelop of the reactors being converted.

Keywords

U-10Mo, Fuel Qualification, United States High Performing Research Reactors

Nomenclature

ATR	Advanced Test Reactor
ATR-C	Advanced Test Reactor Critical Facility
DNBR	Departure from Nuclear Boiling Ratio
DOE	United States Department of Energy
DOE-NE	United States Department of Energy, Office of Nuclear Energy
DOE-SC	United States Department of Energy, Office of Science
EFPD	Effective Full Power Day
EOL	End of Life
FCI	Fuel-Cladding Interactions
FIR	Flow Instability Ratio
FSP	Full Sized Plate
GTRI	Global Threat Reduction Initiative
ICPMS	Inductively Coupled Plasma Mass Spectrometry
HEU	Highly Enriched Uranium
HFEF	Hot Fuel Examination Facility
HFIR	High Flux Isotope Reactor
HIP	Hot Isostatic Press
HPRR	High Performance Research Reactor
LEU	Low-Enriched Uranium
LWR	Light Water Reactor
M^3	Material Management and Minimization
MCNP	Monte Carlo N Particle
MIT	Massachusetts Institute of Technology
MITR	Massachusetts Institute of Technology Reactor
MP	Miniature Plate
MURR	University of Missouri Research Reactor
NIST	National Institute of Standards and Technology
NBSR	National Bureau of Standards Reactor
NNSA	National Nuclear Security Administration
NRC	Nuclear Regulatory Commission
ORIGEN	Oak Ridge Isotope Generator
PIE	Post Irradiation Examination
RERTR	Reduced Enrichment for Research and Test Reactors Program
SFT	South Flux Trap
USHPRR	United States High Performance Research Reactor Project

1. Introduction

The United States High Performance Research Reactor (USHPRR) project is conducting a fuel qualification and licensing campaign focused on converting high power research reactors in the US from the use of high-enriched uranium (HEU) to low-enriched uranium (LEU) (<20% ^{235}U enrichment) fuel forms. The project addresses the fuel conversion of domestic reactors regulated by both the United States Nuclear Regulatory Commission (NRC) and the Department of Energy (DOE) (see Table 1). Therefore, dissemination of detailed qualification and licensing processes is also beneficial to entities seeking licensing of new commercial nuclear fuel forms, including advanced reactor fuels and accident tolerant light water reactor (LWR) fuel candidates.

Table I. Reactors and Critical Assemblies to be Converted from HEU to LEU in the USHPRR Program.

HPRR	Location	Regulatory Agency
Massachusetts Institute of Technology Nuclear Research Reactor (MITR)	Massachusetts Institute of Technology (MIT)	NRC[1]
University of Missouri Research Reactor (MURR)	University of Missouri	NRC
The National Bureau of Standards Reactor (NBSR)	National Institute of Standards and Technology (NIST)	NRC
The High Flux Isotope Reactor (HFIR)	Oak Ridge National Laboratory (ORNL)	DOE-SC[2]
The Advanced Test Reactor (ATR)	Idaho National Laboratory (INL)	DOE-NE[3]
The Advanced Test Reactor Critical Facility (ATR-C)	Idaho National Laboratory (INL)	DOE-NE

[1] U.S. Nuclear Regulatory Commission (NRC)
[2] U.S. Department of Energy, Office of Science (DOE-SC)
[3] U.S. Department of Energy, Office of Nuclear Energy (DOE-NE)

No suitable LEU fuel is currently available to enable conversion of these reactors. Therefore, USHPRR is working towards (a) qualifying a high-density LEU fuel for the reactors specified in Table I, (b) commercializing fuel fabrication processes and inspection methods, and (c) supporting the modification of codes and methods used in analyzing reactor safety in support of licensing. The fuel qualification effort undertaken in USHPRR is far too broad and detailed for one single technical publication. This paper summarizes the previous fuel qualification efforts by the Reduced Enrichment for Research and Test Reactors (RERTR). The four main objectives of this work are describing the selected high-density LEU fuel, defining the general approach used to progress the selected U–10Mo fuel design through the first stage of generic fuel qualification, and managing the miniature fuel test plate irradiation campaign.

1.1 Background of U-10Mo Monolithic Fuel

USHPRR had successfully converted most research reactors as part of the silicide campaign. As part of this campaign multiple versions of silicide fuels were hypothesized and tested [1-5]. As part of the U.S. Nuclear Regulatory Commission technical report designation (NUREG) 1313 silicide elements were given permission for insertion and eventual conversion [6,7]. However, silicide fuels were not in contention as a fuel choice for the five high performance research reactors and critical assembly due to limitations on operating capabilities. Initially a U-Mo dispersion fuel was down selected as a potential candidate through irradiation of the experiments RERTR 1-6. U-Mo dispersion fuel performed as expected in mini-plate tests [8-17]. European full sized plates indicated that porosity formed at the fuel/matrix interface, which was seen in previous RERTR tests would lead to breakaway swelling in plates of prototypic geometries, but under similar conditions U-10Mo monolithic continued to exhibit stable behavior during irradiation. This represented a divergence in the US and European qualification efforts, as the US began to shift focus to U-10Mo monolithic. Starting with RERTR-7, fabrication methods were more heavily scrutinized, and RERTR-7 tested friction stir welding methods of fuel fabrication. Additionally, these plates had 58% U-235 enrichment, and were subjected to 90 effective full power days, which achieved over 100 at% LEU depletion, RERTR-8 represented the first time the monolithic plates were fabricated using the hot isostatic press technique. RERTR-9 tested the effect of modified fuel-cladding interfaces to mitigate the effect of the interaction layer between the fuel and cladding at greater than 90 effective full power days. The monolithic plates were tested with a Zr diffusion barrier between the cladding and fuel or thin layers of silicon between the fuel and cladding [18]. RERTR-10 further tested the interlayers that were proposed during RERTR-9. Furthermore, the manufacturing techniques of hot isostatic pressing and friction bonding were compared [19]. RERTR-12 tested the selected U-10Mo monolithic fuel with a co-rolled zirconium interlayer, clad in aluminum 6061 via hot isostatic press tested at a range of fission densities and fission rates. Specimens used HEU fuel to achieve relatively high fission rates. Pillowing was observed on several mini-plates but they were all on plates where fission densities which exceeded fission densities possible in an LEU fuel. RERTR-12 marked the end of the U-10Mo monolithic fuel development phase.

2. Irradiation Test Design for U-10Mo Fuel to Support Qualification

With the development and demonstration of U-10Mo monolithic fuel as a viable high-density, LEU fuel, evaluation of core conversions for the US HPRRs began. Ultimately U-10Mo monolithic fuel was chosen for conversion of the Advanced Test Reactor (ATR), Advanced Test Reactor Critical Facility (ATR-C), National Bureau of Standards Reactor (NBSR), University of Missouri Research Reactor (MURR), and Massachusetts Institute of Technology Nuclear Research Reactor (MITR). A roadmap and plan were laid out to accomplish the following: transfer

the fuel fabrication process to a commercial fuel fabricator, test commercially fabricated fuel (mini-plate, full size plates, and elements) to support a generic fuel qualification, and ultimately demonstrate the fuel with irradiation tests designed to mimic conversion elements for each reactor. The MP-1 irradiation campaign is the first irradiation of commercially fabricated U-10Mo monolithic fuel. It acts as a bridge between fuel development and fuel qualification with plates fabricated using the laboratory-scale fuel fabrication process and the commercial scale fabrication processes. The specimens in MP-1 bound power and fission densities expected in the three NRC regulated US HPRRs; MITR, NBSR, and MURR. Data from MP-1 will be used to measure fuel performance and material properties post-irradiation and compare to measurements taken on as-fabrication characterization samples. Fuel performance metrics such as stable and predictable behavior, geometric stability, and mechanical integrity.

2.1 Description of U-10Mo Monolithic Fuel

The selected LEU fuel for conversion of most of the US HPRRs is a U-10Mo monolithic fuel plate with a Zr diffusion barrier clad in Al-6061, illustrated below in Fig. 1. The Zr diffusion barrier reduces the detrimental fuel-cladding interactions (FCI) between the U–Mo fuel and the Al-6061 cladding to avoid formation of undesirable microstructural features which can lead to unstable fuel performance behavior during irradiation [20]–[22].

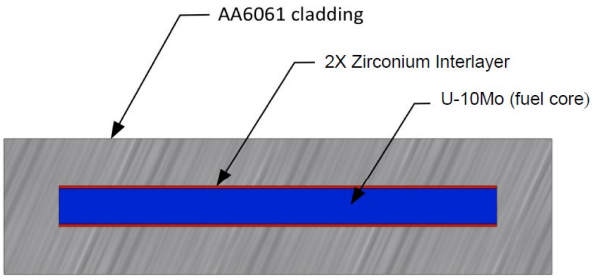

Fig. 1 Illustration of the high-density U-10Mo LEU fuel plate.

The maximum theoretical density of the U-10Mo is about 17.2 $g \cdot cm^{-3}$. The monolithic fuel form is preferred over its dispersion form due to the higher fuel core density. U-10Mo was shown to be more thermodynamically stable and have superior irradiation performance compared with U-7Mo during historical irradiation testing [23]. Many U-10Mo thermophysical properties have been established from previous research, including heat capacity, coefficient of thermal expansion, thermal diffusivity, and thermal conductivity [24]. While previous tests have been performed to understand the irradiation behavior and stability of this LEU fuel system [23, 25], formal generic fuel qualification of the commercially fabricated fuel under an established quality program must be completed before proceeding to reactor conversions.

2.2 MP-1 Test Design

The MP-1 experiment was initially conceptualized and designed as a fabrication down select experiment focused on zirconium interlayer application methods. The purpose was to test commercially fabricated fuel with different zirconium interlayer applications, in prototypic reactor environments. Ultimately, the project selected co-rolling of the Zr as the preferred fabrication method, due to the maturity of the technology, which changed the objective of the MP-1 experiment from down select to one of confirming that the commercial process meets the established performance requirements [26]. In addition to the commercially fabricated specimens, reference plates were included in the MP-1 experiment design to provide a link to irradiation performance data previously generated by the program. These were fabricated using the same general process as RERTR-12 mini-plates tested during the fuel development phase of the project. The chosen fabrication method is a monolithic U-10Mo fuel core, hot co-rolled with a zirconium diffusion barrier to form the fuel foil that is then clad in aluminum 6061 using hot isostatic pressing (HIP).

3. MP-1 Design Approach

MP-1 is the first of a series of tests that seeks to irradiate mini-plates that bound operating ranges of research reactors. These reactors include MURR, MITR, NBSR, ATR, and ATR-C and do not include HFIR, as the experiment is not designed to use a silicide fuel that would emulate the chosen conversion fuel for HFIR. In general, USHPRR experiments are required to reach what are considered bounding conditions plus a suitable margin for normal operations, and these conditions are specific to the reactor in question.

The first step in the design process is to identify conditions to be tested. LEU core designs were evaluated and sub-tests within the experiment were defined. Fuel and cladding thickness were assessed and plates with the greatest fuel thickness and thinnest cladding were grouped. Bounding operating conditions for these plates were gathered. Representative fuel and cladding thickness and irradiation targets were then selected to represent these plates. Plates that experience the highest burn up, tracked as fission density which is independent of enrichment or fissions of other heavy metal atoms [27], were then grouped and representative geometry and irradiation conditions were chosen. The resulting targets for MP-1 are shown in Table II. Target 1 plates are called MP-1 low power and target 2 plates are called MP-1 medium power. Figure 2 shows the element design of the reactors whose conditions are included in MP-1. Initial MP-1 design included a high power sub-test that utilized HEU fuel to achieve conditions relative to ATR high power operations. Due to complications of utilizing HEU fuel, this scope was removed from MP-1 and moved into a future test called MP-ATR. Hereafter, only the low and medium power MP-1 subtests will be discussed.

With the planned geometries and the targets determined, modeling and simulation of the neutron transport and isotope generation and depletion within the experiment was used to identify irradiation positions and capsule loadings necessary to achieve power density targets. Proposed designs were iterated with thermal hydraulic modeling to determine if a proposed

design would fall within fuel safety limits and ATR safety requirements. Once an acceptable design was proposed the length of irradiation was determined to yield the desired end of life fission density.

Table II. Fuel characteristics and target irradiation conditions,

Bounding Plate		MURR 22	MITR 4 and 16	MURR 1	NBSR 1
Thicknesses, cm (in.)	**Fuel**	0.0508 (0.020)	0.0635 (0.025)	0.023 (0.009)	0.0216 (0.0085)
	Cladding	0.0305 (0.012)	0.0305 (0.012)	0.0445 (0.0175)	0.0533 (0.021)
	Plate	0.112 (0.044)	0.124 (0.049)	0.112 (0.044)	0.127 (0.050)
Peak Power Density, kW/cm^3		7.4	1.7	14.4	11.2
Peak Fission Density, × 10^{21} f/cm^3		2.1	1.97	3.37	6.2
Category		Greatest fuel foil thickness/ thinnest cladding		Highest fission density	
Target		1		2	
Thicknesses, cm (in.)	**Fuel**	0.0635 (0.0250)		0.0216 (0.0085)	
	Cladding	0.0305 (0.012)		0.0508 (0.020)	
	Plate	0.124 (0.049)		0.124 (0.049)	
Target Power Density kW/cm^3		7.7		17.6	
Target Node Size	**W × L cm**	0.5 × 2.54	(MURR)	0.5 × 2.54	(MURR)
		1.32 × 3.16	(MITR)	2 × 2	(NBSR)
Target Fission Density, × 10^{21} f/cm^3		2.5		6.45	

The design of the mini-plates and the mini-plate capsules was developed during prior irradiation tests. An eight-plate capsule design was selected for MP-1 and hafnium rings were incorporated into the lower power capsules to reduce corner peaking in the mini-plates. Edge and corner peaking occurs when flux from the reactor and flux born within the fuel combine at the edges of the fuel resulting in higher localized fission rates. Corner peaking is particularly challenging in mini-plates because of their small size relative to the test position meaning corners will occur at peak flux locations within test positions. Hafnium rings were used to reduce this effect but only in the low power plates. The design target for the medium power plates have corner peaking in the represented plates, thus corner peaking was planned into the MP-1 medium power design. Fig. 2 gives a detailed view of the MP-1 capsules. Four mini-plate capsules are stacked to create a single test train.

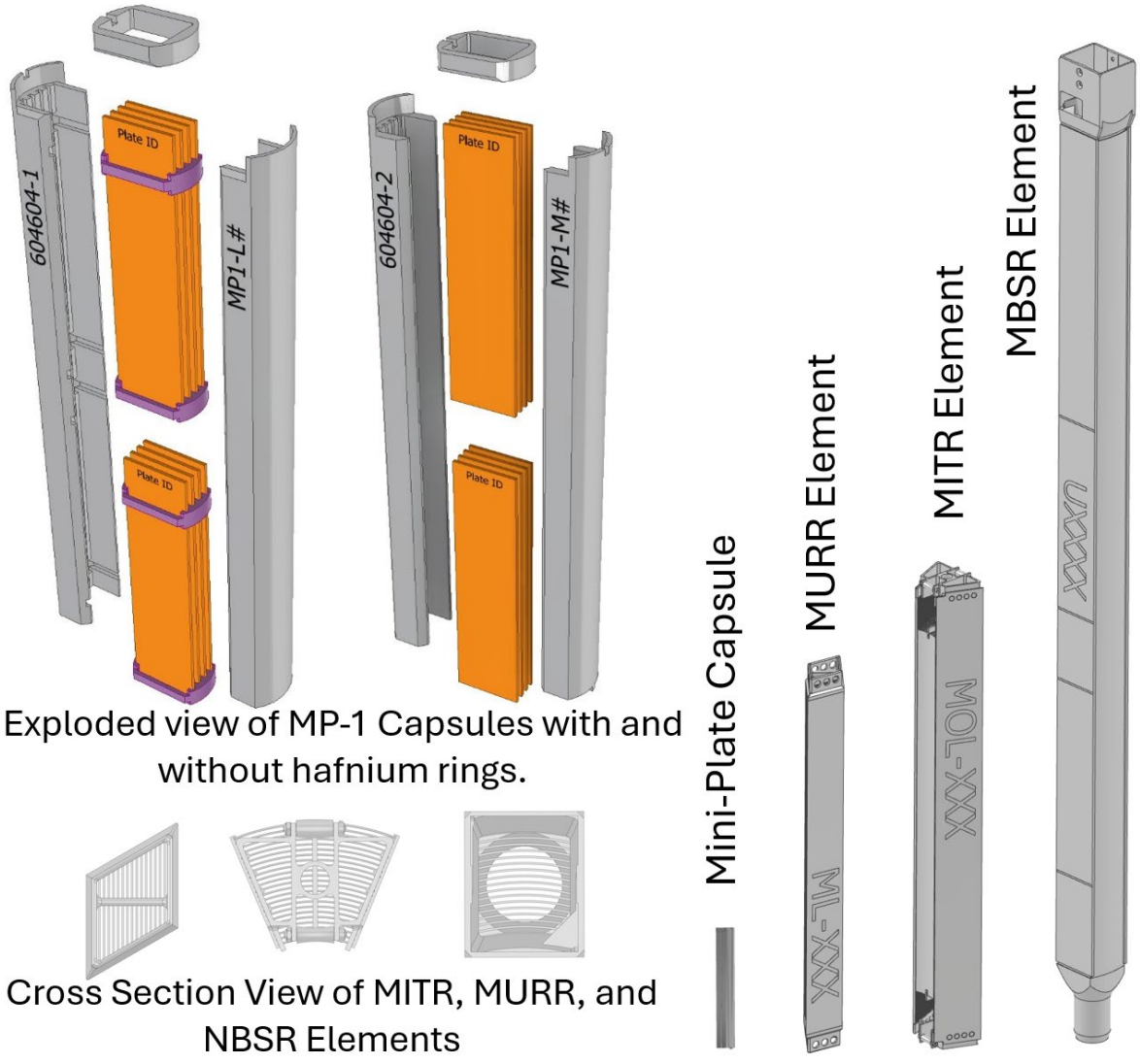

Fig. 2. MP-1 mini-plate capsule design details and comparison to reactor elements.

3.1 MP-1 Meshing Methodology

The MP-1 conditions are designed to match power and fission density targets of the specific reactor. Because the mini-plate is so small compared to actual fuel elements, a meshing scheme is used to correlate fuel volume in a mini-plate to the volume of an analysis node in the LEU conversion core models for the reactors of interest. To model this, each mini-plate in the MP-1 experiment was subdivided such that the axial and transverse mesh was 4×16. These nodal positions all have the same fuel thickness, so the thickness of the mesh is uniform across all voxels. As a result of splitting each mini-plate into a 4×16 mesh, each voxel was 0.516 (axial) × 0.476 (transverse) × fuel thickness cm. Within this mesh, each mini-plate had a different region of

interest or node, which is determined by the reactor of interest. These regions, called reactor nodes, can be seen in Fig. 3. This is designed to ensure that there is a comparison between mini-plates and the analysis node dimensions of actual reactor fuel plates.

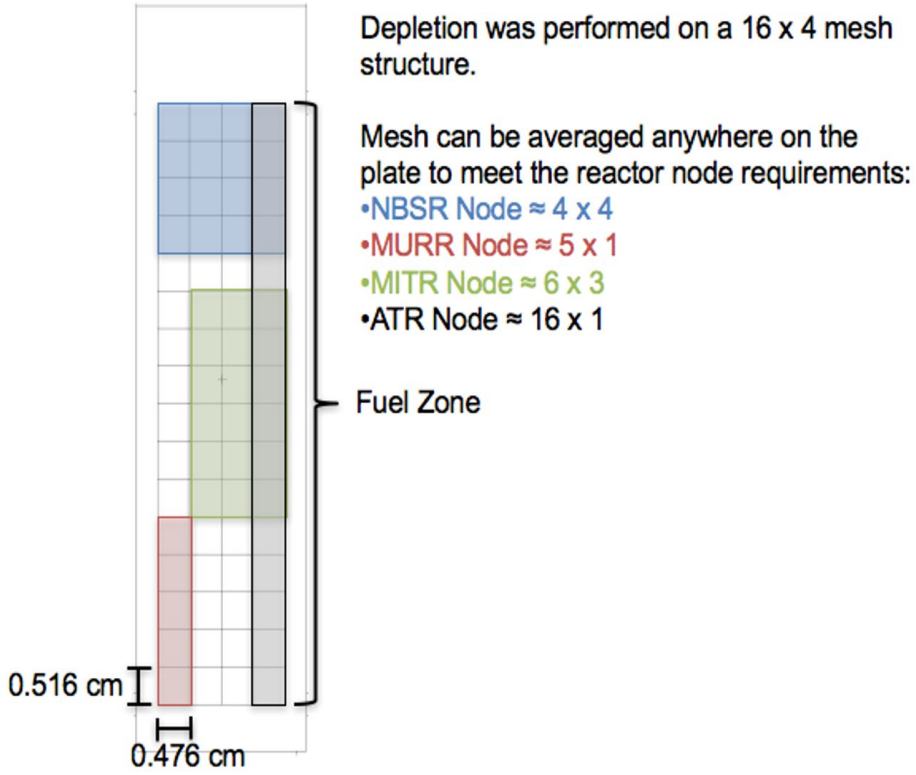

Fig. 3. Nodal regions for each of the reactors of interest for all mini-plates for all of the reactors USHPRR is planning on converting. Note that while an ATR node is shown MP-1 does not encompass ATR irradiation tests.

To acquire nodal data, a user defined mesh is applied. This mesh corresponds to where post irradiation examination data is acquired. This process does not use the inbuilt Monte Carlo N Particle (MCNP) mesh functions, such as Tmesh of Fmesh, but rather are user defined cells. This allows for individual tallies and material definitions to be applied to each voxel. However, to determine if a mini-plate met the requirements outlined in Table II, a series of averaging schemes was applied for both fission and power density. Mini-plate nodes were averaged to match the reactor node size shown in Fig. 3. The averaged region was shifted over the entire area of the mini-plate to identify the peak for both fission and power density for the fuel volume of interest for the entire plate. For example, for an NBSR mini-plate, the peak power and fission density were found by averaging the power density and fission density within the 4x4 mesh. To determine the peak plate condition the same process was executed by applying the region of interest over the next sets of nodes, and the highest of the four node averages was the peak plate condition. This was to ensure that the mini-plate node matched with a similar fuel volume of an actual fuel plate of the respective reactor, so a comparison could be made.

3.2 MP-1 Power Density Methodology

To predict the conditions that any experiment achieves within ATR, modeling is required. The suite of tools used for this predictive modeling is MCNP 5 and Oak Ridge Isotope Generator (ORIGEN) 2 [28], [29]. MCNP is a Monte Carlo program that simulates the transport of neutrons through a series of probability density functions. This program is useful in simulating individual particle tracks and recording, in a tally, their average behavior. The ATR MCNP is a 3D model with a fixed source definition, which means the fission source term is explicitly defined in the source definition card. Thus, to determine neutron specific information such as flux or fission heating, MCNP is utilized to determine these parameters through the f4 cell flux tally and a f7/f6 fission heating tally/energy deposition tally. Since MCNP utilizes normalized flux and fission heating data, a reactor power correction is necessary to achieve physical results. For an f4 tally of neutrons, a reactor power correction was made by understanding the relationship between overall core power, the recoverable energy from fission neutrons, and the average number of neutrons per fission. This correction is outlined in Eq. 1,

$$\emptyset_{neutron} = \frac{\nu \, \emptyset_{MCNP} \, P}{E_R} \tag{1}$$

Where ν is the average number of neutrons per fission, E_R is the energy recovered from a given fission event in joules, P is power in Watts, and φ_{MCNP} is the MCNP cell neutron flux. Note, that this correction did not include an eigenvalue correction, because models used a fixed source approach which obviates the need for an eigenvalue correction.

Outside of f4 tallies, which is utilized primarily for approximating experiment neutron fluxes, MCNP is useful in providing information regarding particle heating parameters such a fission and gamma heating. This parameter, similar to the neutron flux, is dependent upon the mini-plate mesh. The fission heating tally was applied to each voxel shown in Fig. 4. Each cell averaged value yields a different volumetric heat source, which is important when determining whether the experiment met the power density requirements and the efficacy of cooling regimes within the experiment test train. To calculate the power density derived from the experiment, an f6 or f7 tally is used. For MP-1, the f7 tally was utilized to generate prompt gamma and neutron heating into a power density term for each voxel. The MCNP default units for an f7 tally are in MeV g^{-1} n^{-1} so a power correction, identical to a cell flux tally is applied to scale the results with reactor power. This correction can be seen in Eq. 2,

$$E_{deposition}(neutron/photon) = \frac{\nu \, F7_{MCNP} \, P}{E_R} \tag{2}$$

where the units of $E_{deposition}$ tally are in W/g. To determine the power density in a node, the power corrected f7 tally is multiplied by the fuel mass and divided by the volume of the voxel. The averaging scheme noted in 3.1 was applied to determine the peak value and location for a given reactor node.

In addition to the prompt effects of fission and subsequent gamma release, the gamma decay of fission products does contribute to the overall heat density albeit less than prompt heating. MP-1 incorporated delayed photon heating parameters into the predictive modeling. To accomplish a delayed photon correction, a modified form of Eq. 2 is utilized and shown in Eq. 3.

$$E_{deposition}(\text{delayed gamma}) = \frac{\gamma\ F6_{MCNP,delayed\ photon}\ P}{E_R} \quad (3)$$

The difference between the delayed and the prompt contributions, is that the source definition is altered such that delayed photon source emissions and associated probabilities are utilized, and instead of 2.43 neutrons per fission as a normalization constant, a constant (γ) value of 8.9603 photons per fission is used. These terms are applied by utilizing the delayed fission product gamma yield spectrum from either an ATR fuel element or from the zero power physics reactor experiments. Once the volumetric heat source from the delayed photon contribution is known the total heat source term is calculated by summing the contributions from prompt neutrons, prompt photons, and delayed photons. The sum is utilized as the volumetric heat source term for thermal calculations.

3.3 MP-1 Fission Density Methodology

The CINDER-90 module within MCNP can provide detailed depletion information, but the main challenge to using the module is the inability to do a nodal burn analysis, which is used in USHPRR experiment analysis within the burn card, there is not an option to assign an isotope inventory analysis to a specific cell. Since each node was created by manually modeling the cartesian mesh, it is not trivial to assign a burnup analysis. In addition, a power fraction is required to be input into a burn card. This parameter is difficult to ascertain due to the burn analysis being done upon an experiment instead of a reactor element, where the effective power is relatively constant as a function of time. In the experiment the effective power will drop over time due to the loss of fissile material number density and the buildup of poisons. This parameter can be approximated by volume integrating the neutron flux in the mesh nodes, the amount of energy released per fission event, and the overall macroscopic fission cross section. However, this procedure requires an MCNP simulation before a burn analysis could be completed, which then requires another MCNP simulation to procure the depletion information.

Therefore, to increase the efficiency of data collection, ORIGEN was used to determine the depletion parameters. ORIGEN is a deterministic program that solves a series of first order, linear Bateman equations using inbuilt matrix solvers with data from ATR specific cross section libraries, or user defined 1-group cross sections. User defined 1-group microscopic cross sections are required if experiments contain significant amounts of neutron absorbing material. If the user chooses to define the microscopic group cross section, input group cross sections are determined by MCNP a priori through a series of tally multiplier functions that yield reaction rate data divided by the neutron flux as shown in Eq. 4.

$$\sigma_m = \frac{C \int \emptyset(E) R_m(E) dE}{\emptyset(E)} = \frac{F4\ _{with\ tally\ multiplier}}{F4} \quad (4)$$

The variable C is a constant multiplier set to one and $R_m(E)$ is the reaction type of interest.

The next input that is needed for ORIGEN is a power corrected flux that is acquired from Eq. 1. This flux data is read into a script that will apply a further power correction that considers the position of the shims and control drums. This is needed to account for nonlinear effects such as albedo or regions of strong absorption. For USHPRR experiments, the overall depletion is defined as the time integral of the fission rate density not the amount of energy extracted per mass of heavy metal. Note, that the fission density is also mesh dependent, so ORIGEN calculates the depletion and isotope inventory for each mini-plate node. Once the depletion is complete for a given time step, the chemistry is inserted into the MCNP material card of the experiment. This allows for a new flux spectrum and energy deposition to be simulated using new experiment chemistry, and the process iterates until the end of life depletion conditions for the specific reactor bounds are met. To validate experiment modeling, flux wires are irradiated with experiments to measure reactor flux as a function of experiment position. These values are then used to adjust the predictive modeling if necessary as part of an "as run" analysis.

3.4 Thermal Analysis

After neutronics calculations are performed, they must be coupled to thermal analysis to determine appropriate flow rates, temperature profiles, and departure from nucleate boiling limits. For flow rate calculations, analytical models are used, but temperature profiles and departure from nucleate boiling ratio (DNBR) limits require the use of a finite element analysis program such as ABAQUS. ABAQUS utilizes the volumetric heat source data from MCNP and data from the analytical models. The overall process for modeling the behavior of the flow and temperature profiles relies upon modeling assumptions. The two primary assumptions are related to the oxide layer that grows during irradiation, and the degradation of thermal conductivity as a function of burnup. The pre-irradiation oxide layer is set at 2 micron, and growth of this layer is determined using the modified Griess correlation. The U-10Mo thermal conductivity degradation correlation is outlined in the U-10Mo Fuels Handbook [30].

3.4.1 Analytical Thermal Analysis

To determine the velocity of water flowing through an experiment at the ATR, a few key assumptions must first be made. One, the overall allowed pressure drop through the experiment is determined by how many pumps are operating during the cycle. For MP-1 a normal two pump 60-day operation cycle was utilized. This correlates to a maximum allowable pressure differential of 77 psi. This change in pressure correlates to a velocity of fluid by utilizing the mechanical energy balance in Eq. 5.

$$V = \sqrt{\frac{2\,\Delta P + \rho g\,\Delta h}{\rho\left(K_c + K_e + K_f\right)}} \tag{5}$$

The variable V is velocity, ΔP is core pressure drop, ρ is coolant density, K_c is loss coefficient due to contraction, K_e is loss coefficient due to expansion, and K_f is loss coefficient due to wall friction.

The pressure drop limit for experiments is approximately 77 psi for ATR two-pump operation. USHPRR analysis also ignores the contribution from hydrostatic pressure ($\rho g\, \Delta h$) as this contributes less than 2 psi. Density is evaluated at 125°F and 360 psig (reactor core inlet temperature and pressure). The contraction loss coefficient K_c and the expansion loss coefficient K_e are assumed to be 0.5 and 1.0 respectively. These values were not calculated for MP-1, but rather were constants from tables in fluids textbooks such as Munson et. al [31]. However, the friction loss coefficient K_f, which is geometry dependent, for MP-1 was determined by utilizing a friction factor-Reynolds number correlation. The correlation used in MP-1 was the empirical Zigrang-Sylvester approximation to the Colebrook-White equation, which explicitly defines the Darcy-Weisbach friction factor instead of using Moody friction charts. This correlation is applicable for both smooth and rough pipes within a turbulent flow regime. This correlation is outlined in Eq. 6.

$$\frac{1}{\sqrt{f}} = -2\log_{10}\left\{\frac{\varepsilon}{3.7D} + \frac{2.51}{Re}\left[1.14 - 2\log_{10}\left(\frac{\varepsilon}{D} + \frac{21.25}{Re^{0.9}}\right)\right]\right\} \tag{6}$$

The variable f is the Darcy-Weisbach friction factor, ε is wall roughness, D is hydraulic diameter, and Re is Reynold's number. However, this is not the overall loss coefficient. Once the Darcy-Weisbach friction factor was known, K_f could be found explicitly using Eq. 7.

$$K_f = \frac{f\, L}{D} \tag{7}$$

The variable L is the length of the flow channel and D is the hydraulic diameter. Once the friction loss coefficient is known, the fluid velocity through the MP-1 experiment was calculated using Eq. 6. Note, that these equations have nonlinear relationships between Reynolds number, Darcy-Weisbach friction, and the friction loss coefficient. To balance this, MathCad R15 solved these equations, iteratively, by assuming a velocity, calculating the respective Reynold's number, Darcy-Weisbach friction factor, and using the resulting loss coefficients into the mechanical energy balance equation until the assumed velocity corresponded to the calculated velocity.

When using convective cooling, a known heat transfer coefficient is required. Ultimately, there are many methods to calculate a heat transfer coefficient, but the correlations that empirically determine the coefficient vary in accuracy. The heat transfer coefficient is calculated using Eq. 8.

$$h = \frac{Nu\, k}{D} \tag{8}$$

The parameter D is the hydraulic diameter, which is a known parameter, and k is thermal conductivity. The parameter Nu is the Nusselt number, which is found through empirical correlations with varying degrees of applicability depending on parameters such as Reynold's number, the ratio of channel length to hydraulic diameter, or Prandtl number. The most common of these Nusselt correlations is the Dittus-Boelter correlation, which could within some degree of accuracy provide a reasonable heat transfer coefficient for use in determining the overall plate surface temperature along with the temperature of the fluid within the flow channels. However,

USHPRR used the Gnielinski correlation for MP-1 as it provides a more accurate Nusselt number compared with power correlations such as Dittus-Boelter or Seider-Tate [32]. The Gnielinski correlation is shown in Eq. 9,

$$Nu = \frac{\frac{f}{8}(Re - 1000)Pr}{1 + 12.7\left(\frac{f}{8}\right)^{\frac{1}{2}}\left(Pr^{\frac{2}{3}} - 1\right)} \tag{9}$$

where f is the Darcy friction factor defined by Petukhov's correlation, and Pr is the Prandtl number. The Prandtl number is the ratio of kinematic viscosity to thermal diffusivity, and both parameters can be found using fluid property handbooks such as those generated by the National Institute of Standards and Technology [33]. These parameters do vary as a function of temperature, so, to account for this, all properties are evaluated at the oxide film temperature. This temperature is defined as the simple average of the wall temperature and the bulk fluid temperature.

3.4.2 Thermal Analysis Using ABAQUS

Once the analytic and neutronics calculations are completed for an experiment, these are read into ABAQUS to calculate thermal safety parameters and temperature profiles. For the MP-1 experiment, ABAQUS utilized the 20 × 40 mesh, which is different than the mesh for power density outlined in section 3.3. To counteract this, an integration scheme is used to interpolate the power density between the voxels of the neutronics mesh, such that an ABAQUS equivalent voxel power density is obtained. Each voxel's power density represents, in ABAQUS, a unique volumetric heat source. ABAQUS solves a 3-D Fourier heat conduction law problem for steady state conditions, and a transient version of the Fourier heat conduction law, which is described in Eqs. 10–11.

$$\nabla^2 T + \frac{\dot{q}}{k} = \frac{1}{\alpha}\frac{dT}{dt} \tag{10}$$

For steady state,

$$\nabla^2 T + \frac{\dot{q}}{k} = 0 \tag{11}$$

T is the temperature, $\dot{q}$ is the volumetric heat, k is thermal conductivity, and α is the thermal diffusivity However, to visualize the process for solving fuel centerline for MP-1, a 1-D steady state model is described to highlight the equations and procedure for solving the finite element solution. The 1-D centerline temperature for an aluminum-clad fuel with prescribed volumetric heat generation being cooled by water as shown in Fig. 4.

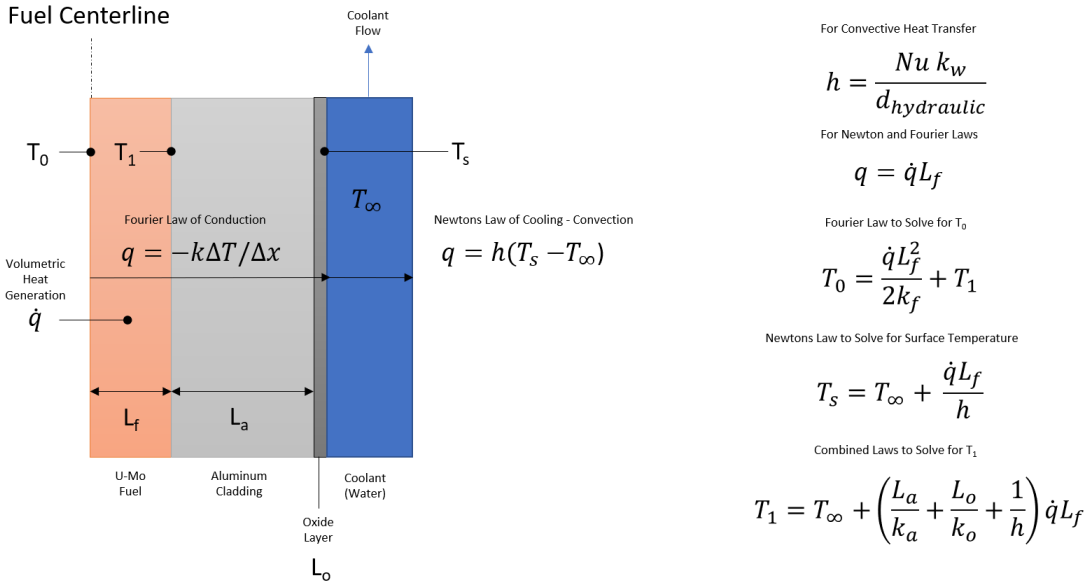

Fig. 4. 1D representation of heat transfer of the MP-1 Monolithic plates cooled by water.

One-dimensional steady state heat conduction in ABAQUS solves a series of heat balance equations, specifically for boundary heat fluxes. For the plate surface temperature interacting with the working fluid, Newton's cooling law was utilized to ascertain the temperature. The fuel centerline temperature requires Fourier's heat conduction law. For the aluminum cladding, a resistance term is utilized to determine the boundary temperature between the fuel and cladding. This resistance term is shown in Eqs. 12-13.

$$q = \frac{\Delta T}{\Sigma R} \tag{12}$$

Where,

$$\Sigma R = \frac{L_a}{k_a} + \frac{L_o}{k_o} + \frac{1}{h} \tag{13}$$

q is the heat flux, the resistance term R is based upon the geometry of the system, ΔT is the temperature difference between the boundary of the cladding/fuel and the temperature of the fluid, and k is the thermal conductivity of the media. The general solutions to these equations are shown in Fig. 4. It should be noted that the zirconium diffusion barrier was not included in the thermodynamic analysis and is defined as aluminum. The thickness of the zirconium is very thin (~0.001 in.) in comparison to the thickness of the fuel and cladding and does not contribute significantly to the temperature difference at that interface for steady-state analyses. The thermal effects of the interlayer being modeled as aluminum are within the margin of error (~2%) for the analysis using the most extreme heat flux in the plates.

Since ABAQUS utilized a finer version of the MP-1 neutronics mesh defined in section 3.3, this methodology was repeated for all ABAQUS voxels, and temperatures for each of the surfaces were calculated. With these surface and interface temperatures known, the oxide layer expansion was calculated using the modified ATR Griess correlation, shown in Eq. 15. The oxide growth is an important phenomenon to model, because of the feedback loop that is created. As oxide layer thickness increases the convective heat transfer coefficient decreases, which causes plate surface temperature to increase. This causes an acceleration of oxide layer growth. These phenomena are shown in Eqs. 14–15,

$$t_{oxide} = 17.8 \cdot 443 \cdot \theta^{0.778} \cdot \exp\left(\frac{-4600}{T_s}\right) \tag{14}$$

where t_{ox} is the thickness of the oxide layer in microns and θ is the time in hours. The corrected heat transfer coefficient shown in Eq. 16. Was updated for each depletion step and reallocated within ABAQUS.

$$h_{tot} = \frac{1}{\frac{1}{h} + \frac{t_{oxide}}{k_{oxide}}} \tag{15}$$

Since the working fluid interacts with the oxide layer, the addition of oxide growth must be accounted for as the increase in oxide thickness reduces cooling from convection while acting as an insulator on the cladding surface. This oxide growth, if uncontrolled, could cause overheating during a volatile transient.

For transient cases, ABAQUS calculations included the material specific heat to calculate the stored energy at each node for each time increment; the transient equation is shown in Eq. 9. Transient calculations are used when calculating heat flux and temperatures for reactivity insertion accident evaluations, which is the limiting accident scenario for ATR experiments. These equations, both steady state and transient, were solved by using the Newton-Raphson nonlinear iterative method.

Note, the models used in ABAQUS are nonlinear because the material properties and the convective heat transfer coefficients are dependent on temperature. Parameters are corrected as the irradiation simulation progresses. The strategy above is repeated over the life cycle of the experiment. Thermal conductivity degrades as fission density increases. As a result of fuel swelling, hydraulic diameter changes which degrades convective cooling properties [34]. Each of the aforementioned equations are recalculated for each timestep, using input from the prior timestep, MCNP and ORIGEN, then used as the inputs to the next set of calculations. This provides a quasi-time dependent simulation through the irradiation cycles.

3.5 Preliminary Safety Analysis

In addition to showing programmatic targets are met, various safety calculations are required for the ATR safety analysis. These include reactivity and temperature coefficient calculations in the physics analysis as well as quantifying the impact of the experiment on the surrounding fuel element. Various thermal calculations and provided to show cooling time requirements and temperatures during reactor accidents. Structural calculations are performed to show the experiments fall within plant requirements. These details of these safety calculations are not included in this document. However, an often-limiting safety metric that requires consideration during design is DNBR and flow instability ration (FIR). Thus, these will be discussed in more detail.

Before an experiment is given approval for insertion into the ATR, the experiment must prove that it has adequate cooling. This requirement necessitates a DNBR and flow instability ratio (FIR) analysis to assure the experiment has sufficient margin to avoid a film boiling condition during normal and off-normal reactor operating conditions. To achieve sufficient DNBR margin, all experiments are required to have a DNBR greater than 2.0 for both steady state and transient conditions. DNBR is a ratio of the critical heat flux to the local heat flux, shown in Eq .16.

$$DNBR = \frac{q_{crit}}{q_{local}} \tag{16}$$

Since ATR coolant is subcooled and MP-1 experiment cladding was aluminum, the critical heat flux was approximated using the Savannah River correlation shown in Eq.17 [35].

$$q_{chf} = 1.88\, x10^5(1.0 + 0.0515\, V)(1.0 + 0.069\, \Delta T) \tag{17}$$

For this correlation, V is velocity in ft/sec, ΔT is the coolant subcooling in °F, and q_{chf} is in BTU hr^{-1} ft^{-2}. The DNBR was evaluated where the subcooling is minimized, and this generally occurs at the channel outlet of the experiment. ABAQUS provides the local heat fluxes for the steady state cases, and for transient cases to generate the ratios.

Another safety parameter that is important to experiment safety is the FIR. Flow instability represents a departure from a single phase and introduces flow abnormalities such as the introduction of voids and bubbles. Similar to DNBR, FIR must also always be above 2.0 for experiments. FIR, shown in Eq. 18, is a ratio of the temperature rise to saturation to maximum temperature rise of the primary coolant along the flow channel.

$$FIR = \frac{T_{sat} - T_{inlet}}{X(T_{local} - T_{inlet})} \tag{18}$$

If both ratios are greater than 2.0, then the experiment is allowed for insertion into the ATR.

4. Irradiation Experiment Design

Four experiment positions were identified for the MP-1 experiment. Low power targets were identified in three large B positions, B-10, B-11, and B-12, and South Flux Trap (SFT) was identified for the medium power targets. Initially, various fabrication methods were to be tested, which required a high number of samples. A design was proposed in which all low power plates and all medium power plates reached the same end of life fission density. When the fabrication variable was cut down to only commercial versus laboratory fabrication, it allowed the irradiation durations to be adjusted to achieve not only bounding but also intermediate fission densities. The as-designed beginning of life power densities and end of life fission densities for the MP-1 experiment are summarized below in Fig. 5 and will be detailed in the forthcoming sections.

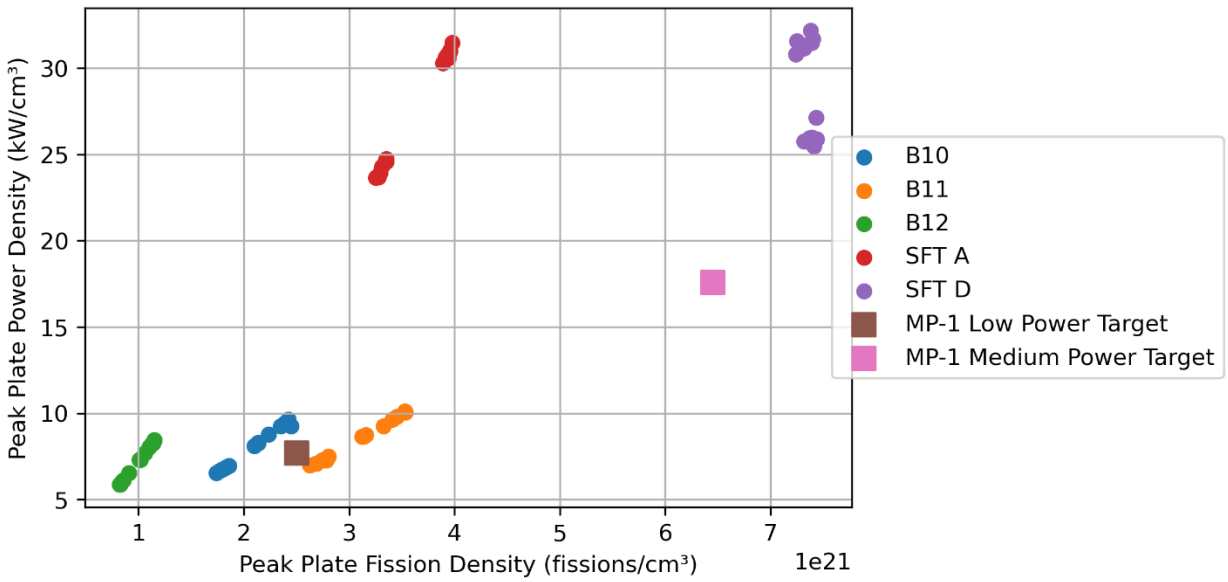

Fig. 5.Design irradiation conditions in the MP-1 experiment compared to the low and medium power targets.

4.1. Low Power Irradiation Test

The low power irradiation sub-test aims to reach a nominal power target of 7.7 $kW \cdot cm^{-3}$, representative of MURR 22/MITR 4 and 16. Each mini-plate test train, shown below in Fig. 6 will contains up to 32 plates; however, 18 of these positions will be occupied by dummy aluminum plates during irradiation. Also shown in Fig. 6 are the hafnium rings which will be used as burnable absorbers to suppress excess reactivity peaking in the mini-plates. A total of 42 fueled plates will be irradiated in the ATR as part of the low power sub-test. Each individual test train will be placed inside of large B positions (B-10, B-11, and B-12) in such a way that the IDs of the plates will be facing core center (i.e., in face-on orientation), as illustrated in Fig. 7. The main advantage of irradiating plates in such orientation compared to edge-on in large B positions—where the neutron

flux gradient is significant in the radial direction—is that mini-plates achieved more uniform power distribution, which is more representative of the large-size plates. The plates in the low power test will be cooled by the primary reactor coolant during irradiation. It is planned to remove fueled capsules from B-12 and B-10 positions after 1 and 2 irradiation cycles, respectively, so that the plates can achieve intermediate levels of burnup. Plates in B-11 position will be withdrawn after 3 cycles, after they achieve final target burnup.

The low power plates are predicted to exceed beginning of life power density and end of life fission density, which is deemed to be bounding. Thermally, the low power tests are predicted to have a fuel centerline temperature of 134 °C at the B-10 position, 137 °C at the B-11 position, and 124 °C at the B-12 position during normal operations. These meet the limit of being less than 360°C, which is less than the lowest blister threshold temperature measured for U-10Mo monolithic fuel [36]. The temperature profiles do grow oxide on the aluminum cladding. The predicted oxide growth for the low power tests varies by position. In B-10 the peak thickness is 25.0 μm, in B-11 the peak thickness is 25.8 μm, and in B-12 the peak thickness is 23.1 μm. However, the temperature difference across the oxide layer is less than 119 °C in all cases [36]. This means that spallation of the boehmite pre-film will not occur. In terms of flow stability and DNBR, Each of these tests satisfies the requirement that these values must always be greater than two. For the low power case in the most limiting ATR accident scenario, the minimum DNBR was 2.04 which occurred in the B-10 position. Minimum FIR occurred in B-11 with a predicted value of 3.56.

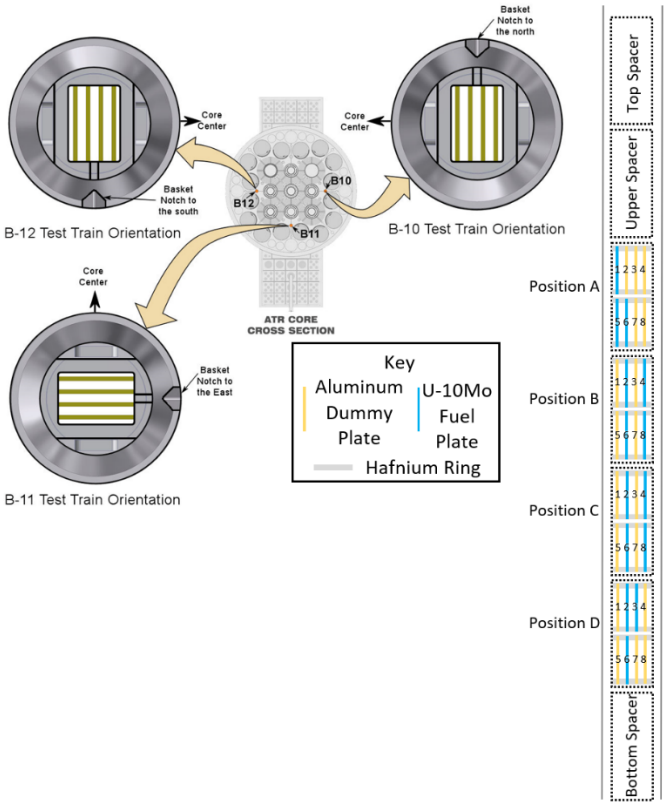

Fig. 6. Illustration of the ATR core showing the B-10, B-11, and B-12 irradiation positions to be used for the mini-plate low power tests.

4.2. Medium Power Irradiation Test

Thirty-two fuel specimens were designed in medium power (17.6 $kW \cdot cm^{-3}$) conditions representative of MURR 1/NBSR 1 in the arrangement illustrated in Fig. 7. Hafnium neutron flux suppressors will not be utilized in this configuration because corner peaking in the mini-plates is prototypic of corner peaking in the limiting NBSR plate. The test train will be placed inside of the ATR's SFT in such a way that the IDs of the plates will be facing east of the reactor core (see Fig. 7). Because the SFT position is surrounded by ATR driver fuel, the mini-plates in the edge-on configuration in SFT will achieve more uniform power distribution as compared to mini-plates in face-on configuration in large B test positions which are located further away from the ATR driver fuel. To achieve target fission density, mini-plates in capsules D (see Fig. 7) will be irradiated for 6–8 cycles. Fuel plates in capsules A will be removed midway through irradiation to achieve intermediate level of burnup. The plates will be cooled by the primary reactor coolant during irradiation.

The medium power plates are predicted to exceed beginning of life power density and end of life fission density. Thermally, the medium power tests are predicted to have peak fuel centerline temperatures of 123°C which is below the blister threshold temperature of U-10Mo fuel. The peak

oxide thickness is expected to be 12.8 μm. The maximum temperature gradient across the oxide layer in the medium power plates is 40.27 °C which is below the oxide spallation temperature of 119 °C. The design of MP-2 medium power test trains is expected to have a minimum DNBR of 2.2 and FIR of 3.3.

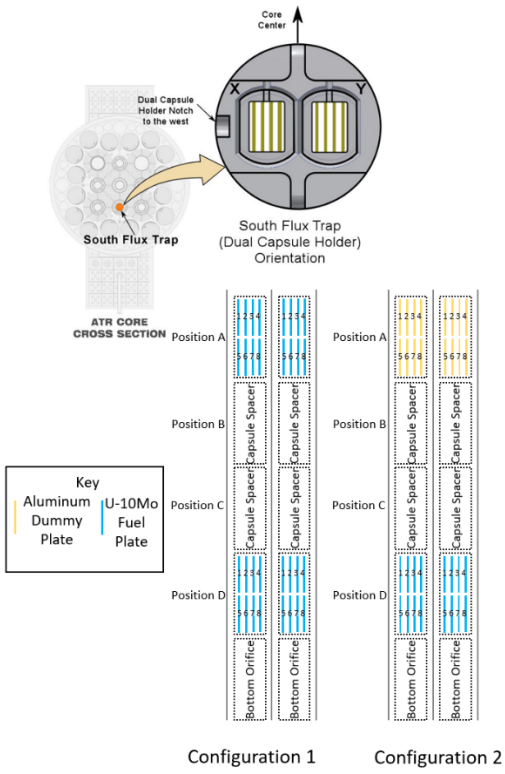

Fig. 7. South Flux Trap dual-channel capsule holder showing the location of the 32 fuel mini-plates for the medium power irradiation test.

5. Conclusions

This manuscript outlines the process utilized in the development of fuel qualification tests undergone by USHPRR to demonstrate that U-10Mo monolithic is a viable fuel alternative to current HEU fuels. MP-1 is the first in a series of tests designed to demonstrate the efficacy of the fuel. LEU designs of three USHPRRs were used to identify target conditions for the irradiation test. Per the modeling methodology MP-1 meets or exceeds the minimum requirements set by the individual reactors to verify similar performance of U-10Mo to the current regime of HEU oxide dispersed fuel. Additionally, MP-1 passes the baseline safety requirements imposed by the ATR. The next step for MP-1 is to irradiate the experiment and conduct post irradiation examination to supply data for the subsequent experiments that USHPRR has planned. Subsequent tests include a larger mini-plate test to gather statistically relevant performance data over a wider range of irradiation conditions and fuel thicknesses. Full-plates and element tests will also be designed and irradiated to support generic qualification of the U-10Mo monolithic fuel system.

Declaration of Competing Interest

On behalf of all authors, the corresponding author states that there is no conflict of interest

Acknowledgements

This work was supported through the U.S. Department of Energy National Nuclear Security Administration under the United States High-Performance Research Reactor Project and DOE Idaho Operations Office Contract DE-AC07-05ID14517. Accordingly, the U.S. Government retains and the publisher, by accepting the article for publication, acknowledges that the U.S. Government retains a nonexclusive, paid-up, irrevocable, world-wide license to publish or reproduce the published form of this paper, or allow others to do so, for U.S. Government purposes.

References

[1] D. C. Crawford, D. L. Porter, S. L. Hayes, M. K. Meyer, D. A. Petti, and K. Pasamehmetoglu, "An approach to fuel development and qualification," *J. Nucl. Mater.*, vol. 371, no. 1–3, pp. 232–242, 2007, doi: 10.1016/j.jnucmat.2007.05.029.

[2] K. A. Terrani *et al.*, "Accelerating nuclear fuel development and qualification: Modeling and simulation integrated with separate-effects testing," *J. Nucl. Mater.*, vol. 539, p. 152267, 2020, doi: 10.1016/j.jnucmat.2020.152267.

[3] IAEA, "Good Practices for Qualification of High Density Low Enriched Uranium Research Reactor Fuels," *IAEA Nucl. Energy Ser.*, no. No. NF-T-5.2, p. 74, 2009.

[4] D. LANNING, D.D., LEWIS, R.A., STAHL, "National plan for development of high uranium density research and test reactor fuel to accommodate use of low uranium enrichment," 1977.

[5] R. . HOFMAN, G.L., NEIMARK, L.A., MATTAS, "Irradiation behaviour of miniature uranium silicide fuel plates," in *IAEA*, 1982, pp. 88–98.

[6] *Safety evaluation report related to the evaluation of low-enriched uranium silicide-aluminum dispersion fuel for use in non-power reactors*. United States: N. p., 1988. Web. doi:10.2172/6830338.

[7] L. A. HOFMAN, G.L., NEIMARK, "Irradiation behaviour of uranium-silicide dispersion fuels," in *Intl Mtg on RERTR*, 1984, pp. 45–53.

[8] J. . COPELAND, G.L., HOFMAN, G.L., SNELGROVE, "Examination of U3Si2-Al fuel elements from the Oak Ridge Research Reactor," in *Intl Mtg on RERTR*, 1986, pp. 211–221.

[9] Nuclear Regulatory Commission DC (USA) Office of Nuclear Reactor Regulation, "Safety evaluation report related to the evaluation of low-enriched uranium silicide-aluminum dispersion fuel for use in non-power reactors," no. July, p. 119, 1988, [Online]. Available: http://inis.iaea.org/search/search.aspx?orig_q=RN:20012810.

[10] M. K. Meyer *et al.*, "Low-temperature irradiation behavior of uranium-molybdenum alloy dispersion fuel," *J. Nucl. Mater.*, vol. 304, no. 2–3, pp. 221–236, 2002, doi: 10.1016/S0022-3115(02)00850-4.

[11] D. M. Wachs, "RERTR Fuel Development and Qualification Plan," January, 2007.

[12] M. K. Meyer, G. L. Hofinan, R. V Strain, C. R. Clark, and J. R. Stuart, "Metalographic Analysis of Irradiated RERTR-3 Fuel Test Specimens," 2001.

[13] S. L. Hayes, M. K. Meyer, T. C. Wiencek, J. R. Stuart, and P. I.G., "Prototypic irradiation testing of high-density U-Mo alloy dispersion fuels," in *Intl Mtg on RERTR*, 1999, no. October 3-8.

[14] G. L. Hofman, M. K. Meyer, and J.-M. Park, "Observation on the Irradiation Behavior of U-Mo Alloy Dispersion Fuel," 2000, [Online]. Available: https://inis.iaea.org/collection/NCLCollectionStore/_Public/42/024/42024794.pdf?r=1&r=1.

[15] G. L. Hofman *et al.*, "Recent observations at the postirradiation examination of low-enriched U-Mo miniplates irradiated to high burnup," *Intl Mtg RERTR*, p. 12, 2003.

[16] G. L. Hoffman, J. L. Snelgrove, S. L. Hayes, and M. K. Meyer, "Progress in Development of Low-Eneriched U-Mo Dispersion Fuels," in *Trans. of 2003 International Topical Meeting on Research Reactor Fuel Management*, 2002, pp. 50–58.

[17] G. L. Hoffman, J. L. Snelgrove, H. S.L., M. K. Meyer, and C. R. Clark, "'Progress in Postirradiation Examinination and Analysis of Low-Enriched U-Mo Research Reactor Fuels,'" in *Trans. of the 2003 International Topical Meeting on Research Reactor Fuel Management*, 2003, pp. 43–49.

[18] D. M. Perez, M. A. Lillo, G. S. Chang, G. A. Roth, and N. E. Woolstenhulme, "RERTR-9 Irradiation Summary Report (INL/EXT-10-18421)," May 2011, 2011

[19] D. M. Perez, M. A. Lillo, G. S. Chang, G. A. Roth, and N. E. Woolstenhulme, "RERTR-10 Irradiation Summary Report (INL/EXT-10-18456)," May 2011, 2011.

[20] A. Leenaers, S. Van Den Berghe, E. Koonen, C. Jarousse, F. Huet, M. Trotabas, M. Boyard, S. Guillot, L. Sannen, M. Verwerft, Post-Irradiation Examination of Uranium-7 Wt% Molybdenum Atomized Dispersion Fuel, J Nucl Mater 335(1) (2004) 39-47.

[21] J. Gan, D.D. Keiser, D.M. Wachs, A.B. Robinson, B.D. Miller, T.R. Allen, Transmission Electron Microscopy Characterization of Irradiated U-7mo/Al-2si Dispersion Fuel, J Nucl Mater 396(2-3) (2010) 234-239.

[22] J. Gan, D.D. Keiser, B.D. Miller, A.B. Robinson, J.F. Jue, P. Medvedev, D.M. Wachs, Tem Characterization of U-7mo/Al-2si Dispersion Fuel Irradiated to Intermediate and High Fission Densities, J Nucl Mater 424(1-3) (2012) 43-50.

[23] J. Gan, B.D. Miller, D.D. Keiser, J.F. Jue, J.W. Madden, A.B. Robinson, H. Ozaltun, G. Moore, M.K. Meyer, Irradiated Microstructure of U-10mo Monolithic Fuel Plate at Very High Fission Density, J Nucl Mater 492 (2017) 195-203.

[24] D.E. Burkes, C.A. Papesch, A.P. Maddison, T. Hartmann, F.J. Rice, Thermo-Physical Properties of Du-10 Wt.% Mo Alloys, J Nucl Mater 403(1-3) (2010) 160-166.

[25] J.F. Jue, B.H. Park, C.R. Clark, G.A. Moore, D.D. Keiser, Fabrication of Monolithic Rertr Fuels by Hot Isostatic Pressing, Nucl Technol 172(2) (2010) 204-210.

[26] D. Keiser, J.F. Jue, B. Miller, J. Gan, A. Robinson, J. Madden, Observed Changes in as-Fabricated U-10mo Monolithic Fuel Microstructures after Irradiation in the Advanced Test Reactor, Jom-Us 69(12) (2017) 2538-2545.

[27] M. Meyer, B. H. Rabin, J. Cole, I. Glagolenko, W. Jones, J. F. Jue, D. Keiser, C. Miller, G. Moore, H. Ozaltun, F. Rice, A. Robinson, D. Wachs, W. Williams and N. Woolstenhulme, "Research and Development Report for U-Mo Monolithic Fuel," Technical Report, INL/EXT-17- 40975. Idaho National Laboratory, Idaho Falls/ID., 2016.

[28] A. G. Croff, "ORIGEN2: A Versatile Computer Code for Calculating the Nuclide Compositions and Characteristics of Nuclear Materials," *Nucl. Technol.*, vol. 62, pp. 335–352, 1983.

[29] X-5 Monte Carlo Team, "MCNP-A General Monte Carlo N-Particle Transport Code, Version 5 Volume I: Overview and Theory," 2003.

[30] J. Rest, Kim, Y. Kim, Hoffman, M. Meyer, and S. Hayes, "*U-Mo fuels handboo"k. Version 1.0*. United States:, 2006. doi:10.2172/1335129.

[31] B. Munson, T. Okiishi, W. Huesbch, and A. Rothmayer, *Fundamentals of Fluid Mechanics*, 7th ed. 2013.

[32] D. Taler, "Simple power-type heat transfer correlations for turbulent pipe flow in tubes," *J. Therm. Sci.*, vol. 26, no. 4, pp. 339–348, 2017, doi: 10.1007/s11630-017-0947-2.

[33] E. Lemmon, M. McLinden, and D. Friend, "Thermophysical Properties of Fluid Systems," in *NIST Chemistry WebBook, NIST Standard Reference Database Number 69*, P. Linstrom and W. Mallard, Eds. Gaithersburg MD: National Institute of Standards and Technology.

[34] Kim, Y. S. and Hofman G. L., "Fission Product Induced Swelling of U-Mo Alloy Fuel," Journal of Nuclear Materials 419, pp. 291-301, 2011.

[35] D. H. Knoebel, S. D. Harris, B. J. Crain, and R. M. Biderman, "Forced-convection subcooled critical heat flux. D_2O and H_2O coolant with aluminum and stainless steel heaters." 1973, Accessed: Oct. 11, 2021. [Online]. Available: https://inis.iaea.org/search/search.aspx?orig_q=RN:4079370.

[36] Rabin, B. Preliminary Report on U-Mo Monolithic Fuel for Research Reactors, Idaho National Laboratory, 2017, INL/EXT-17-40975